$g_{9/2}$ isobaric analog resonances in ^{51}Mn

J. Sziklai* and J. A. Cameron
Tandem Accelerator Laboratory, McMaster University, Hamilton, Ontario, Canada L8S 4K1

I. M. Szöghy
Département de Physique, Université Laval, Québec City, Québec, Canada G1K 7P4

(Received 27 January 1984)

Fragments of the $g_{9/2}$ isobaric analog states in ^{51}Mn corresponding to $E_x=4.101$ MeV ($S_n=0.10$) and $E_x=4.155$ MeV ($S_n=0.34$) parent states in ^{51}Cr have been found. To locate the $g_{9/2}$ isobaric analog resonance fragments the ^{50}Cr(p,p$_1\gamma$), ^{50}Cr(p,p$_2\gamma$), and ^{50}Cr(p,γ)^{51}Mn reactions were used. The excitation curves were measured in the $E_p=3.08-3.36$ MeV proton energy range. The excitation function of the (p,p$_2\gamma$) reaction turned out to be a sensitive tool to locate resonances with higher, $\frac{5}{2}\leq J_R\leq\frac{13}{2}$, spins. The spins of the resonances were found using the method of normalized angular distributions. Fifteen $g_{9/2}$ fragments were identified. Partial widths for each fragment and in all three channels were deduced and fine structure analyses were carried out. Inelastic spectroscopic factors and Coulomb displacement energies were derived for both fragmented $g_{9/2}$ isobaric analog resonances. The results were compared with previous work.

I. INTRODUCTION

Analog states appearing in the ^{50}Cr+p system have been investigated extensively by high resolution proton scattering.[1–7] The isobaric analog resonances (IAR's) of the $E_x=4.101$ MeV ($S_n=0.10$) and $E_x=4.155$ MeV ($S_n=0.34$) $1g_{9/2}$ parent states[8,9] have already been identified by Salzmann *et al.*,[3] Whatley *et al.*,[4] and Arai *et al.*[5] There are, however, slight disagreements among the results. Salzmann *et al.*[3] localized three fragments while Whatley *et al.*[4] and Arai *et al.*[5] found only two. None of them found a satisfactory correspondence between the parent and analog states, i.e., the energy difference between the analog states were only about half of that of the parent states. According to the results of Arai *et al.*,[5] a considerable part of the $g_{9/2}$ single-particle strength of the IAR is still missing.

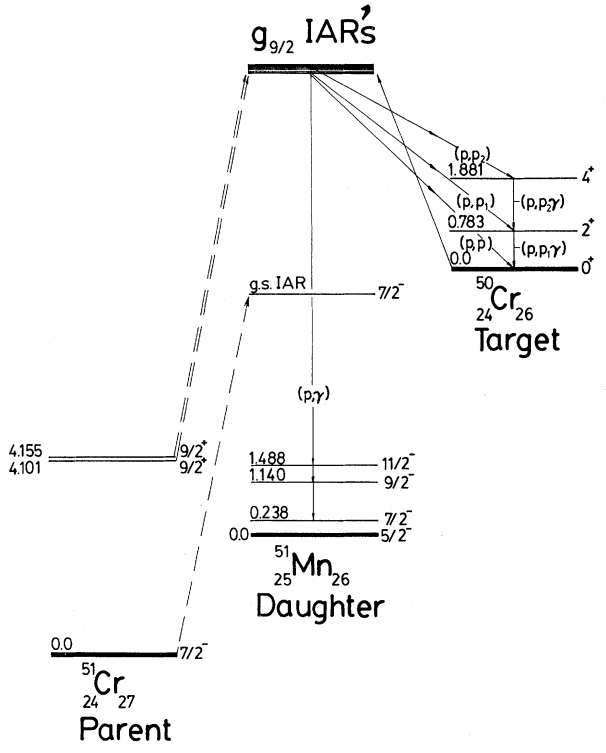

FIG. 1. Schematics of the reactions studied.

Taking into account the relatively large spectroscopic factors of the $1g_{9/2}$ parent states,[8,9] it was expected that their analogs would show interesting features in their γ decay, as it was found in some similar cases.[10–13]

Instead of measuring the angular distributions of the elastically and inelastically scattered protons, reactions involving γ rays, i.e., (p,p$_1\gamma$) and (p,p$_2\gamma$) (see Fig. 1), were used to investigate the resonances. The advantage of the (p,p$_1\gamma$) reaction lies in the fact, that following an inelastic scattering process, the γ decay of the excited states of a medium-heavy target nucleus usually occurs with relatively low energy ($E_\gamma\leq 2.0$ MeV) γ rays. These can easily be detected by Ge(Li) counters or HPGe detectors, with excellent energy resolution and high efficiency. It is therefore possible to obtain a statistically significant γ-ray yield and measure its angular distribution even for weak resonances, thus being able to gain information on their spins.

II. EXPERIMENTAL PROCEDURE

The experiments were begun at the FN Tandem Accelerator of McMaster University with an overall energy resolution of 2.5 keV. The first results showed, however, that a better energy resolution is required for resolving many of the close-lying resonances due to the observed high level density.

The measurements were continued at the 7.5 MV Van de Graaff accelerator of Université Laval, Québec. An overall energy resolution of 1 keV or less was achieved. For brief runs the beam spread was about 600 eV.

The targets were prepared by evaporating isotopically enriched (96.0%) $^{50}Cr_2O_3$ onto thick Ta, Pt, and 40 $\mu g/cm^2$ carbon foil backings. A 12 $\mu g/cm^2$ thick ^{50}Cr target was used for measuring the excitation curves and a 13 $\mu g/cm^2$ thick one was used for the angular distribution measurements. A small tantalum lined reaction chamber of 5 cm radius was used. The elastically scattered protons were monitored by a surface barrier detector, placed at 135° to the beam.

The γ rays were detected by a 26% efficiency (for the 1.333 MeV ^{60}Co line) ORTEC GAMMA-X detector placed at 55° to the beam for measuring the excitation curves and in a 90°-45°-0°-60°-30° cycle for the angular distribution measurements. At −90°, an additional 50 cm^3 Ge(Li) counter was used to monitor the γ-ray angular distributions when thick target backings were used. The data were collected by a PDP-15 on-line computer with four 4096 channel CANBERRA analog to digital converters (ADC's) and were recorded for later analysis.

The excitation curves were measured in the 3.080—3.360 MeV bombarding proton energy range in steps of 600—1200 eV. Typical target current was 0.6—0.9 μA. The charge collected at each step was 0.25 mC.

Reliable angular distribution measurements require knowledge about systematic errors. For this purpose the centering of the beam spot with respect to the detector circle was checked by using a radioactive point source of ^{60}Co and the $E_\gamma = 0.842$ MeV isotropic γ ray from the ^{27}Al(p,p'γ) reaction. Furthermore, the angular distribution measurements on the resonances were repeated in multiple cycles. As a result of the above, the systematic errors were reduced below 2%. The analyses of angular distributions were carried out with the inclusion of both statistical and systematic errors.

III. RESULTS

A. Excitation functions

The excitation functions measured in the $E_p = 3.080$—3.360 MeV bombarding proton energy region in 1.2 keV steps are shown in Fig. 2. Figure 2(a) shows the excitation function of the ^{50}Cr(p,p$_1\gamma$) reaction. Besides the very strong $2d_{5/2}$ IAR fragment (resonance 7, $E_p = 3153.8$ keV), several intense resonances appeared on a very low background, emphasizing the importance of the first inelastic channel in their decay and the negligibility of the contributions arising from Coulomb excitation.

Figure 2(b) shows the excitation function of the ^{50}Cr(p,p$_2\gamma$) reaction. The appearance of the second inelastic channel in the decay of resonances located in the investigated energy region had not been observed before. This is due to the fact that the majority of the experiments, reported on the ^{50}Cr+p system, were of proton scattering type, where, at these relatively low energies, the observation of the (p,p$_2$) channel is very unlikely because

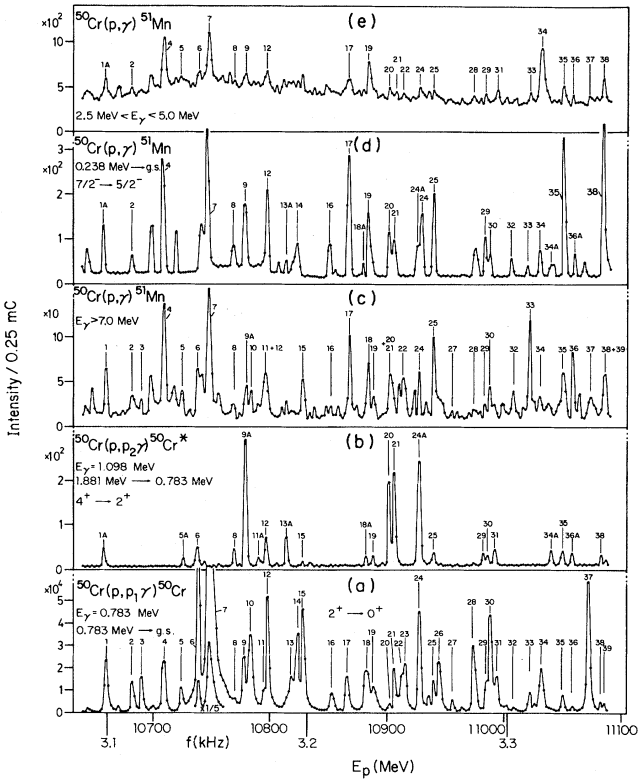

FIG. 2. Excitation functions for the ^{50}Cr(p,p$_1\gamma$), ^{50}Cr(p,p$_2\gamma$), and ^{50}Cr(p,γ)^{51}Mn reactions in the proton bombarding energy region of $E_p = 3.08$—3.36 MeV measured in 1.2 keV steps. The resonances are numbered for easier identification in the text.

of the low penetrability. However, in (^{3}He, d$\tilde{p}$) reactions on other target nuclei Galès *et al.*[14–16] detected coincidence proton groups populating the excited 4^+ states. Unfortunately no such experiment has been reported on ^{50}Cr. The structure of the (p,p$_2\gamma$) excitation curve is much simpler than that of the other channels. The selectivity of the (p,p$_2\gamma$) reaction to the 4^+ state for high spin resonances ($\frac{5}{2} \leq J_R \leq \frac{13}{2}$) is accounted for by the low centrifugal barrier ($l' \leq 2$) in these cases.

Figures 2(c)—(e) show excitation curves of the ^{50}Cr(p,γ)^{51}Mn reaction. Figures 2(c) and (e) are integral excitation functions displaying resonances which populate the low and medium energy levels in ^{51}Mn. Figure 2(d) is a rather rare example of an excitation function for a secondary [$E_x = 0.237$ MeV ($\frac{7}{2}^-$)→g.s. ($\frac{5}{2}^-$)] γ transition reflecting the collection of direct and cascade γ rays originating mostly from higher spin states. The off-resonance population of this first excited state is rather weak, giving a low background for the excitation curve. Since this state has a large spectroscopic factor for proton transfer[17,18] ($C^2S = 0.28$), it contains most of the $f_{7/2}$ single particle strength and is therefore dissimilar to other excited levels of ^{51}Mn. When it is fed directly from IAR fragments, special isospin selection rules[19] apply, i.e., only electromagnetic transitions of $M1$ or $E1$ type are allowed. This means that only IAR fragments having $\frac{5}{2} \leq J_R \leq \frac{9}{2}$ spins and, at the same time, retaining some

single-particle character, are likely to decay directly into this state. Moreover, this is the only known low lying state to which such resonances can decay via isospin allowed $M1$ or $E1$ electromagnetic transitions. If the density of these resonances is much lower than that of the states with more complex nature, its feeding and its subsequent decay to the ground state (g.s.) would appear only at energies where such IAR fragments are excited. The simple low background excitation curve of Fig. 2(d) exhibits this character. According to Noé *et al.*,[20] this $\frac{7}{2}^- \rightarrow \frac{5}{2}^-$ g.s. γ decay has an unusually strong $E2$ enhancement of ~ 47 W.u. This can be attributed to the increased role of configuration mixing and to the structural dissimilarity between the $E_x = 0.237$ MeV level ($C^2S = 0.28$) and the g.s. ($C^2S = 0.03$).

B. Angular distributions and resonance spins

1. Angular distributions of γ rays from the $^{50}Cr(p,p_1\gamma)$ reaction

In order to determine the spins of the resonances, the angular distributions of the 0.7833 MeV γ ray were measured at each observed resonance. For resonances which do not overlap, the pattern of the normalized angular distributions follows those of the theoretical ones. To derive the normalized angular distributions, the normalization factors were first extracted from the intensities observed by the monitor counter: these were simply divided by their mean value for all angles and cycles. The intensities measured with the moving counter were then divided by the corresponding normalization factor and the relative

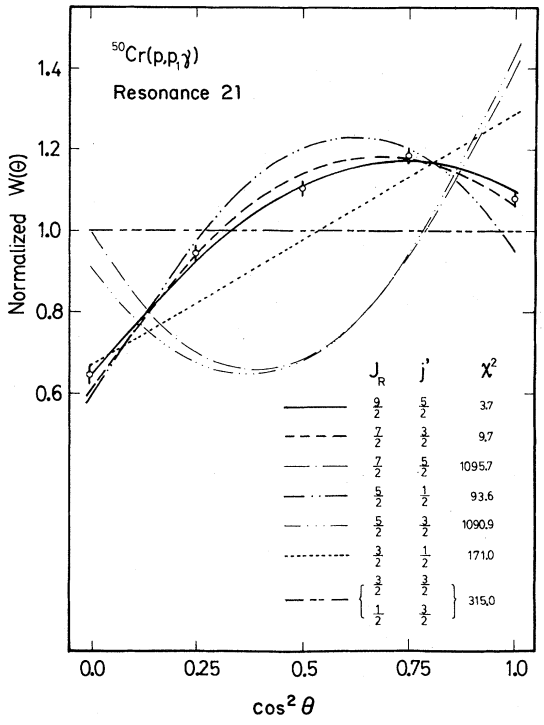

FIG. 3. Fits to the ($p,p_1\gamma$) angular distribution measured at resonance 21. The data are best fitted assuming a $\frac{9}{2}$ resonance spin. The spin selectivity for such isolated resonances was very good. Only the fit made with the right spin assumption gave the reduced χ^2 lower than the selected 0.1% confidence level.

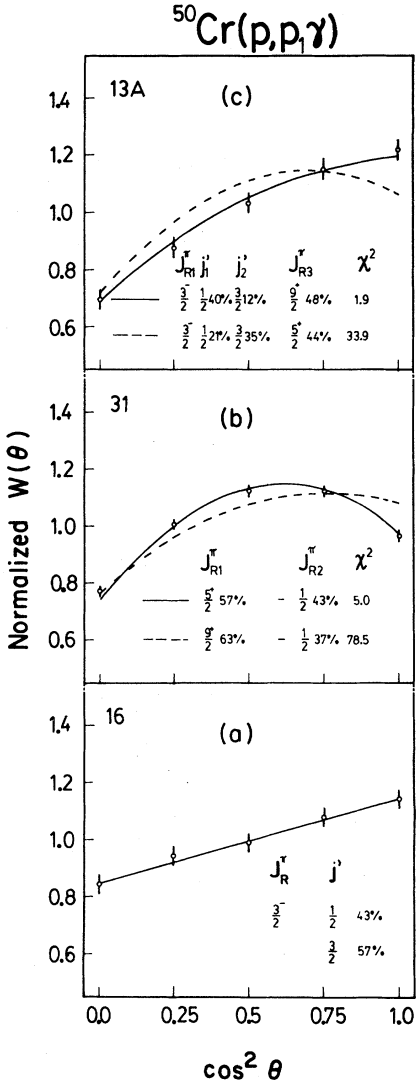

FIG. 4. Examples of analysis of mixed angular distributions. (a) Angular distribution measured at resonance 16. The slight slope of the angular distribution pattern can be explained by supposing a $\frac{3}{2}$ resonance decaying by two $j' = \frac{1}{2}$ and $\frac{3}{2}$ total exit angular momenta. The best fit gave an intensity ratio of $\frac{43}{57}$ for these waves. (b) Angular distribution measured at resonance 31, an example of how one may distinguish between $\frac{5}{2}$ and $\frac{9}{2}$ resonances when a $\frac{1}{2}$ resonance is interfering with the higher spin resonance. The right spin assumption of $\frac{5}{2}+\frac{1}{2}$ (solid line) gives a reduced χ^2 lower than the $\frac{9}{2}+\frac{1}{2}$ assumption (broken line), furthermore, its absolute value falls below the 0.1% confidence level. (c) Angular distribution measured at resonance 18A, an example of a case where a higher spin resonance is mixed with a $\frac{3}{2}^-$ resonance. The best fits with the $\frac{9}{2}+\frac{3}{2}^-$ (solid line) and $\frac{5}{2}+\frac{3}{2}^-$ (broken line) assumptions are shown. The lower reduced χ^2 is obtained for the $\frac{9}{2}+\frac{3}{2}^-$ mixture and its value falls below the 0.1% confidence level.

TABLE I. Resonance spins, exit orbital, and total angular momenta and corresponding penetration factors for the ^{50}Cr(p,p$_1$) reaction [$l' \leq 4$; $E_p = 3.2$ MeV ($2^+ \rightarrow 0^+$)].

J_R^π	l'	j_2'	j_1'	$P(l')$	$\frac{P(l'+2)}{P(l')}$
$\frac{1}{2}^+$	2	$\frac{3}{2}$	$\frac{5}{2}$	1.0×10^{-2}	
$\frac{1}{2}^-$	1	$\frac{3}{2}$		3.7×10^{-2}	
	3	$\frac{5}{2}$		1.2×10^{-3}	0.033
$\frac{3}{2}^-$	1	$\frac{1}{2}$	$\frac{3}{2}$	3.7×10^{-2}	
	3	$\frac{5}{2}$	$\frac{7}{2}$	1.2×10^{-3}	0.033
$\frac{3}{2}^+$	0	$\frac{1}{2}$		8.6×10^{-2}	
	2	$\frac{3}{2}$	$\frac{5}{2}$	1.0×10^{-2}	0.116
	4	$\frac{7}{2}$	$\frac{9}{2}$	1.0×10^{-4}	0.010
$\frac{5}{2}^+$	0	$\frac{1}{2}$		8.6×10^{-2}	
	2	$\frac{3}{2}$	$\frac{5}{2}$	1.0×10^{-2}	0.116
	4	$\frac{7}{2}$	$\frac{9}{2}$	1.0×10^{-4}	0.010
$\frac{5}{2}^-$	1	$\frac{1}{2}$	$\frac{3}{2}$	3.7×10^{-2}	
	3	$\frac{5}{2}$	$\frac{7}{2}$	1.2×10^{-3}	0.033
$\frac{7}{2}^-$	1	$\frac{3}{2}$		3.7×10^{-2}	
	3	$\frac{5}{2}$	$\frac{7}{2}$	1.2×10^{-3}	0.033
$\frac{7}{2}^+$	2	$\frac{3}{2}$	$\frac{5}{2}$	1.0×10^{-2}	
	4	$\frac{7}{2}$	$\frac{9}{2}$	1.0×10^{-4}	0.010
$\frac{9}{2}^+$	2	$\frac{5}{2}$		1.9×10^{-2}	
	4	$\frac{7}{2}$	$\frac{9}{2}$	2.5×10^{-4}	0.013

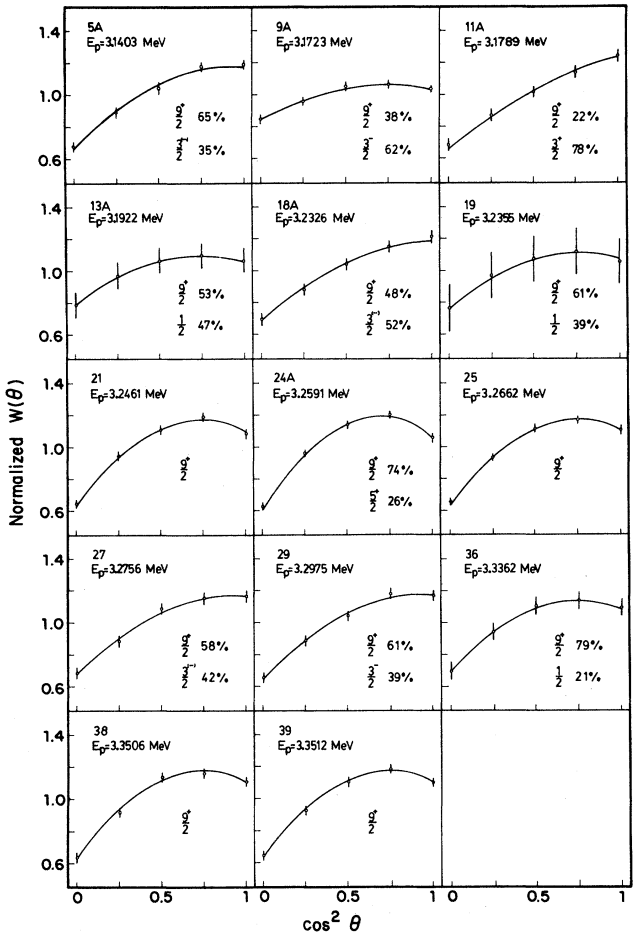

FIG. 5. Angular distributions of γ rays from the ^{50}Cr(p,p$_1\gamma$) reaction for the candidates of $g_{9/2}$ fragments.

efficiency of the moving detector. These normalized angular distributions were then fitted with the theoretical ones, i.e.,

$$W(\theta) = a_0 w(l',j') \,, \tag{1}$$

where

$$w(l',j') = 1 + a_2 Q_2 P_2 + a_4 Q_4 P_4 \,. \tag{2}$$

The a_2 and a_4 coefficients of the Legendre polynomials P_2 and P_4 were taken from the paper of Sheldon and van Patter.[21] The attenuation coefficients were calculated[22] to be $Q_2 = 0.946$ and $Q_4 = 0.840$. The only free parameter for the fits was a_0 (Fig. 3). Only the spin giving the minimum reduced χ^2, and at the same time lower than the selected 0.1% confidence level, was accepted as a possible resonance spin (an example is $\frac{9}{2}$ in Fig. 3).

Of course, due to the relatively high level density and our limited overall energy resolution, many cases were found where the experimentally measured angular distribution patterns were different from the theoretical ones. In these cases our assumptions were as follows:

(i) The resonance has a unique spin but the measured angular distribution is the sum of two angular distributions corresponding to outgoing protons with the same l' but different total angular momenta ($j' = l' \pm \frac{1}{2}$):

$$W(\theta) = a_0[w(l',l'-\tfrac{1}{2}) + \delta_{21} w(l',l'+\tfrac{1}{2})] \,, \tag{3}$$

where $\delta_{21} = I_2/I_1$, i.e., the ratio of the intensities of the two outgoing waves. In our case this sum can be considered to be an *incoherent* one because the outgoing protons were not observed. In these cases a_0 and δ were the free parameters for the fits. This type of analysis [see Fig. 4(a)] can be used generally for resonances with spin parities of $\frac{3}{2}^-$, $\frac{5}{2}^-$, and $\frac{7}{2}^+$, where both of the outgoing waves with $j' = l' \pm \frac{1}{2}$ total angular momenta have the same probability to penetrate the centrifugal barrier (see Table I), thus their mixture is expected in the angular distributions.

(ii) Within our energy resolution unresolved doublets or triplets can be present with different spins and they can decay via protons with $j' = l' \pm \frac{1}{2}$ total angular momenta. The measured angular distributions were fitted with the sum of two [see Fig. 4(b)] or three [see Fig. 4(c)] angular distributions with different resonance spins and total outgoing angular momenta:

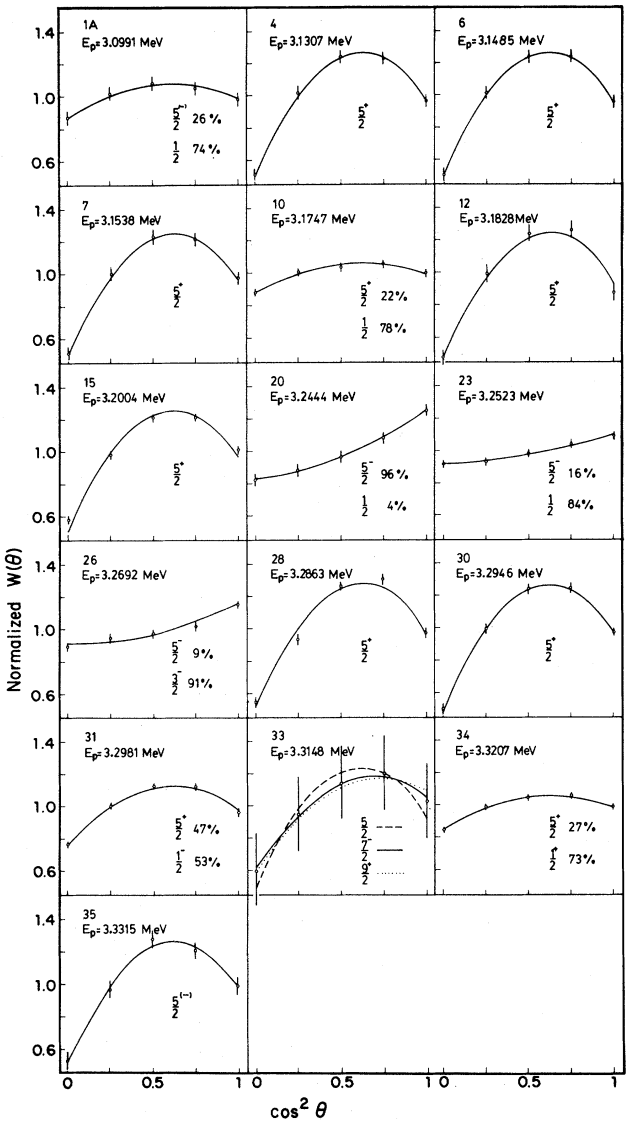

FIG. 6. Angular distributions of γ rays from the ^{50}Cr(p,p$_1\gamma$) reaction for the resonances having spin $\frac{5}{2}$.

$$W(\theta)=a_0[w(l',j')+\delta_{21}w(l'',j'')] \tag{4}$$

or

$$W(\theta)=a_0[w(l',j')+\delta_{21}w(l'',j'')+\delta_{31}w(l''',j''')] , \tag{5}$$

where $\delta_{21}=I_2/I_1$ and $\delta_{31}=I_3/I_1$. In such cases, the free parameters were a_0, δ_{21}, and δ_{31}.

With analyses based on the above equations, we segregated the resonances into two groups: candidates for the $1g_{9/2}$ IAR fragments (Fig. 5) and noncandidates (Figs. 6 and 7). The angular distributions of noncandidates were analyzed, but will be discussed in a separate paper.[23]

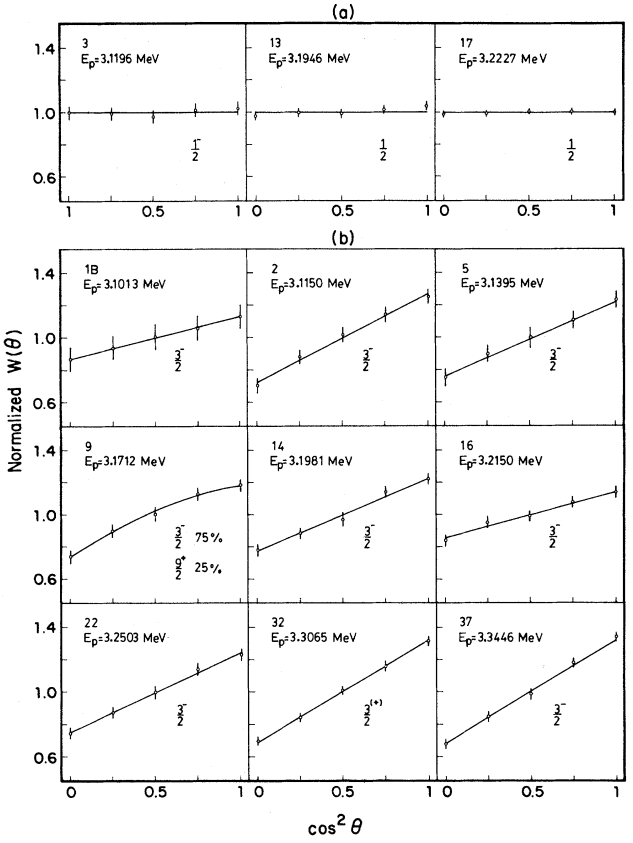

FIG. 7. Angular distributions of γ rays from the ^{50}Cr(p,p$_1\gamma$) reaction for the spin $\frac{1}{2}$ (a) and $\frac{3}{2}$ (b) resonances.

2. *Angular distributions of γ rays from the ^{50}Cr(p,p$_2\gamma$)^{50}Cr* reaction*

The relative intensities of γ rays from the (p,p$_2\gamma$) reaction were at least two orders of magnitude lower than those of the (p,p$_1\gamma$) reaction. Therefore the relative errors in the angular distributions are larger (Fig. 8). In principle it would have been possible to make longer runs in order to improve the counting statistics, but because of the poorer energy stability of the accelerator for extended runs the systematic errors in the angular distributions would also increase.

Unfortunately the angular distribution patterns for this reaction are similar to one another (Fig. 9), thus giving no sharp argument for deciding on the spins. For every $g_{9/2}$ candidate, however, the $J_R=\frac{9}{2}$ spin assumption resulted in the lowest χ^2 for the fits. Generally, they were supportive of the spin assignments based on the analyses of the angular distributions for the ^{50}Cr(p,p$_1\gamma$) reaction.

3. *On the parities*

The (p,p$_1\gamma$) and (p,p$_2\gamma$) angular distributions depend only on the spins of the resonances and not on their parities. There is, however, a limited possibility of inferring

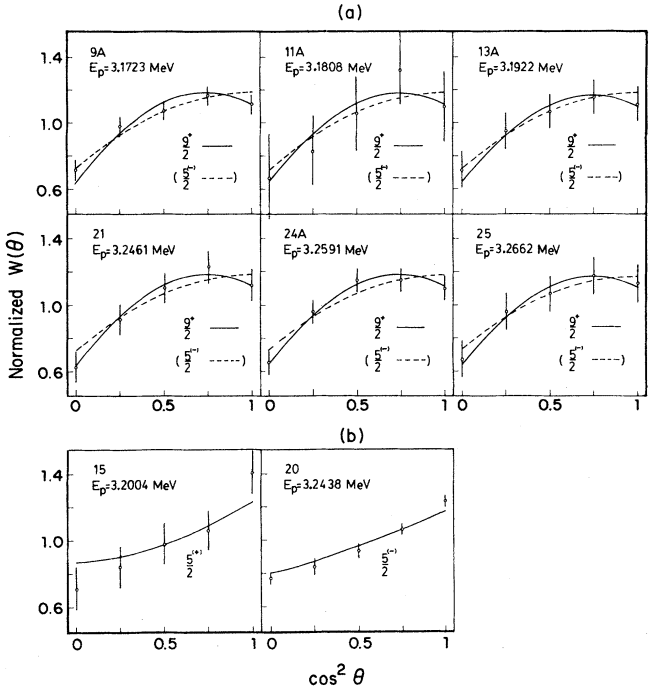

FIG. 8. Angular distributions of γ rays from the ^{50}Cr(p,p$_2\gamma$) reaction for some of the $g_{9/2}$ fragments (a) and for two of the $\frac{5}{2}$ resonances (b).

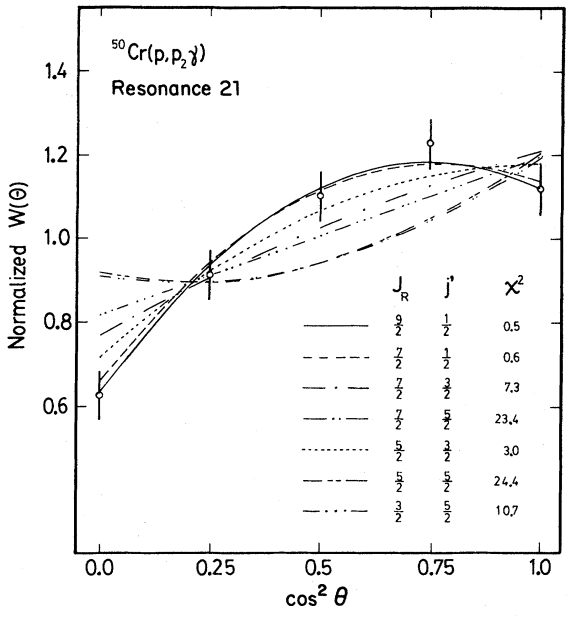

FIG. 9. Fits to the (p,p$_2\gamma$) angular distribution measured, at resonance 21. The analysis cannot give a unique solution, because the assumptions $(J_R;j')=(\frac{9}{2};\frac{1}{2})$, $(\frac{7}{2};\frac{1}{2})$, and $(\frac{5}{2};\frac{3}{2})$ all give reduced χ^2 below the 0.1% confidence level; however, it is consistent with the $\frac{9}{2}$ spin assumption.

the latter through model dependence and kinematic effects.

Table I lists the penetration factors $P(l')$ for different resonances and for all allowed exit l' values for the (p,p$_1\gamma$) reaction. The last column gives the ratios of the penetration factors $P(l'+2)/P(l')$. From this ratio one can infer the relative contributions of different l' in the decay of resonances with different spins and equal partial widths. Resonances with spin parities of $\frac{3}{2}^+$, $\frac{5}{2}^+$, $\frac{7}{2}^-$, and $\frac{9}{2}^+$ are likely to decay by the lowest possible orbital momentum l' and thus only one j' will contribute significantly to the angular distribution as Chou *et al.*[24] found for the $\frac{5}{2}^+$ IAR in ^{49}V. If the contribution of the next higher orbital momentum, $l'+2$, is not, in general, negligible, certainly the contribution of even higher l' values may safely be neglected.

For resonances with spin parities $\frac{3}{2}^-$, $\frac{5}{2}^-$, and $\frac{7}{2}^+$, even the lowest l' values can contribute with total angular momenta $j'=l'\pm\frac{1}{2}$ and it is very likely that their incoherent mixture will appear in the (p,p$_1\gamma$) angular distribution.

Similar conclusions can be made for the (p,p$_2\gamma$) reaction (see Table II) with the difference that resonances with spin parities $\frac{3}{2}^+$, $\frac{5}{2}^-$, $\frac{7}{2}^+$, and $\frac{9}{2}^+$ may give nonmixed

TABLE II. Resonance spins, exit orbital, and total angular momenta and corresponding penetration factors for the ^{50}Cr(p,p$_2$) reaction [$l'\leq 4$; $E_p=3.2$ MeV ($4^+\rightarrow 2^+$)].

J_R^π	l'	j_1'	j_2'	$P(l')$	$\frac{P(l'+2)}{P(l')}$
$\frac{1}{2}^+$	4	$\frac{9}{2}$		2.5×10^{-7}	
$\frac{1}{2}^-$	3	$\frac{7}{2}$		3.4×10^{-6}	
$\frac{3}{2}^-$	3	$\frac{5}{2}$	$\frac{7}{2}$	3.4×10^{-6}	
$\frac{3}{2}^+$	2	$\frac{5}{2}$		5.0×10^{-5}	
	4	$\frac{7}{2}$	$\frac{9}{2}$	2.5×10^{-7}	0.005
$\frac{5}{2}^+$	2	$\frac{3}{2}$	$\frac{5}{2}$	5.0×10^{-5}	
	4	$\frac{7}{2}$	$\frac{9}{2}$	2.5×10^{-7}	0.005
$\frac{5}{2}^-$	1	$\frac{3}{2}$		2.8×10^{-4}	
	3	$\frac{5}{2}$	$\frac{7}{2}$	3.4×10^{-6}	0.012
$\frac{7}{2}^-$	1	$\frac{1}{2}$	$\frac{3}{2}$	2.8×10^{-4}	
	3	$\frac{5}{2}$	$\frac{7}{2}$	3.4×10^{-6}	0.012
$\frac{7}{2}^+$	0	$\frac{1}{2}$		8.0×10^{-2}	
	2	$\frac{3}{2}$	$\frac{5}{2}$	5.0×10^{-5}	0.0006
	4	$\frac{7}{2}$	$\frac{9}{2}$	2.5×10^{-7}	0.005
$\frac{9}{2}^+$	0	$\frac{1}{2}$		8.0×10^{-2}	
	2	$\frac{3}{2}$	$\frac{5}{2}$	5.0×10^{-5}	0.0006
	4	$\frac{7}{2}$	$\frac{9}{2}$	2.5×10^{-7}	0.012

angular distributions, and resonances with spin parities $\frac{3}{2}^-$, $\frac{5}{2}^+$, and $\frac{7}{2}^-$ are likely to give rise to mixed angular distributions.

C. γ-branching ratios of the $\frac{9}{2}^+$ IAR fragments

Because of the weakness of the capture reaction channels no reliable angular distributions could be derived for the primary γ transitions. However, by summing up the spectra measured at different angles, the branching ratios were deduced for some of the $g_{9/2}$ candidates (Fig. 10). The relative errors for the derived branching ratios are from 6% to 11%. Excluding the three high-lying levels of unknown spin ($E_x = 4.153$, 4.532, and 4.776 MeV) only states with spins of $\frac{7}{2} \leq J_f \leq \frac{11}{2}$ were populated. The three levels of unknown spin were populated only in the decay of $g_{9/2}$ resonance candidates. Their subsequent decay to lower-lying states has not been studied. Although the γ decay from the various $g_{9/2}$ fragments does not exhibit a marked similarity, it still supports the spin assignments based on angular distribution measurements.

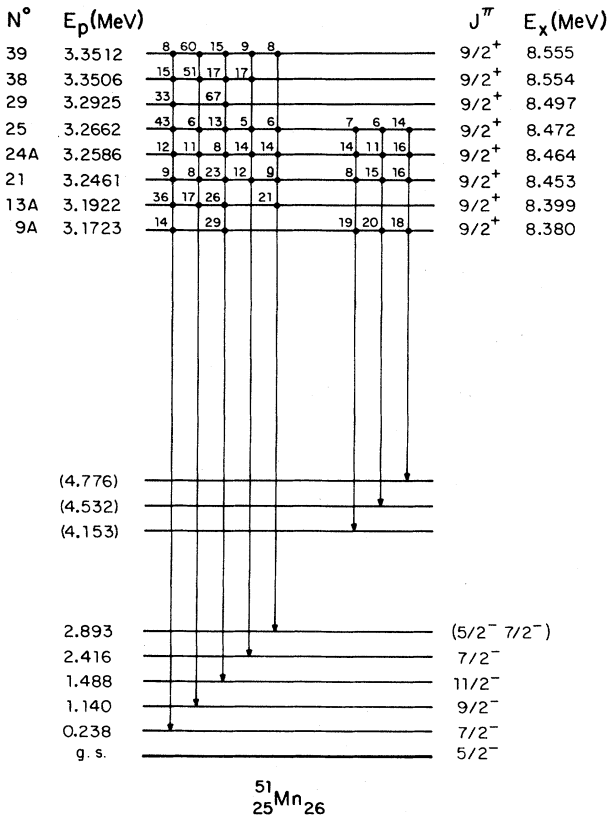

FIG. 10. γ branchings for some of the $g_{9/2}$ candidates. Because of the weakness of the capture channel the branching ratios have errors from 6% to 11%. The energies of levels $E_x = 4.153$, 4.532, and 4.776 MeV may have an uncertainty of ±8 keV, as derived from the γ spectra.

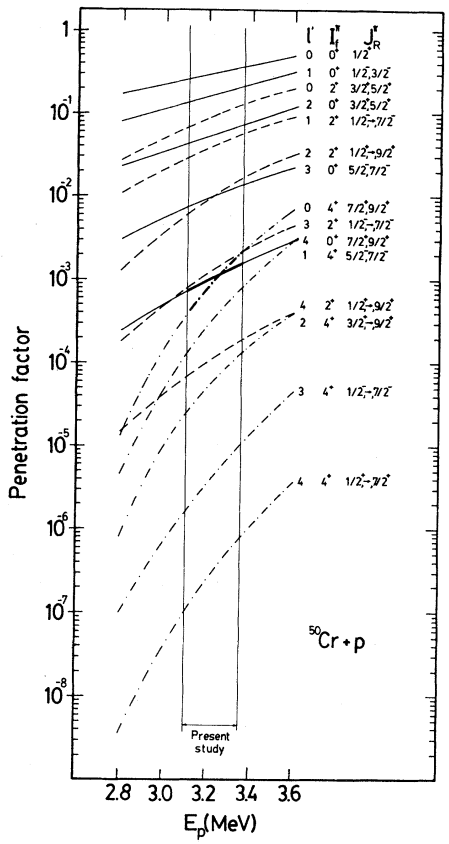

FIG. 11. Penetration factors versus proton bombarding energy for the ^{50}Cr(p,p), ^{50}Cr(p,p$_1$), and ^{50}Cr(p,p$_2$) reactions. The penetration factors in (p,p) and (p,p$_2$) are in the same range (drawn in bold) for resonances with $\frac{9}{2}^+$ and $\frac{7}{2}^+$ spins. Above 3.2 MeV this penetrability for the inelastic protons going to the 4^+ state is higher than that for the elastically scattered protons. Full lines represent penetration factors for protons going to the 0^+ ground state of the target. The dashed and dash-dotted lines are for protons going to the 2^+ and 4^+ excited states, respectively.

IV. THE FRAGMENTS OF THE $1g_{9/2}$ IAR'S

A. Selection of the candidates for the $g_{9/2}$ fragments

Several angular distributions of γ rays from the (p,p$_1\gamma$) reaction measured at the stronger resonances appearing in Fig. 2(a) gave evidence of having important $g_{9/2}$ components. The simple structure of the (p,p$_2\gamma$) excitation function [Fig. 2(b)] and the examination of the ratios of penetration factors for different outgoing partial waves (Fig. 11) feeding different excited states of the target nucleus suggested that there can be other resonances with higher spins, $\frac{5}{2} \leq J_R \leq \frac{9}{2}$. Their intensities turned out to be relatively weak in the (p,p$_1\gamma$) channel. Further angular distribution measurements on these weak resonances or shoulders indeed indicated the presence of such higher spin components. On the basis of the normalized angular distributions it was relatively easy to distinguish between spins $\frac{5}{2}$ and $\frac{9}{2}$ even when resonances of lower spin were present [see, e.g., Figs. 4(b) and (c)].

B. The $g_{9/2}$ resonances

1. $E_p = 3.1403$ MeV, resonance 5A

The $(p,p_1\gamma)$ angular distribution measured on resonance 5 showed a clear $J_R^\pi = \frac{3}{2}^-$ character (Fig. 7) but the angular distribution measured on its high energy shoulder [resonance $5A$ in the $(p,p_2\gamma)$ excitation function in Fig. 2(b)] and an analysis based on Eq. (5) gave indication of a $g_{9/2}$ component. Still, due to our limited overall energy resolution, besides the $g_{9/2}$ intensity the measured $(p,p_1\gamma)$ yield contains about 35% of $\frac{3}{2}^-$ intensity, probably arising from resonance 5.

2. $E_p = 3.1723$ MeV, resonance 9A

This resonance is the strongest one in the $(p,p_2\gamma)$ excitation function [Fig. 2(b)] and does not appear in the $(p,p_1\gamma)$ excitation function [Fig. 2(a)]. However, the $(p,p_1\gamma)$ angular distribution measured on resonance 9 ($J_R = \frac{3}{2}$) has a small but nonvanishing a_4 component (Fig. 7) showing the presence of a close lying resonance with a possible spin of $\frac{9}{2}$. A repeated excitation function measurement with fine 600 eV steps (Fig. 12) shows that this resonance in the $(p,p_1\gamma)$ channel is weaker than the neighboring resonances 9 and 10 and appears between them. The analysis

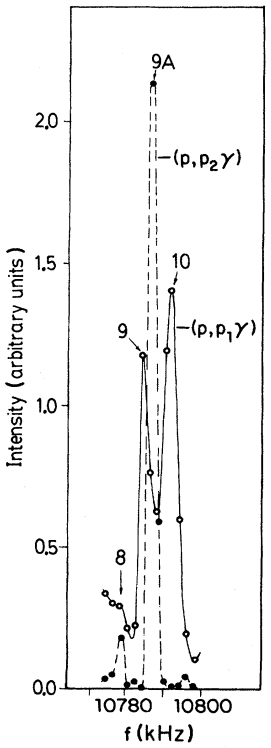

FIG. 12. Differential excitation functions for the ^{50}Cr$(p,p_1\gamma)$ and ^{50}Cr$(p,p_2\gamma)$ reactions measured in 600 eV steps in the vicinity of resonance $9A$. This figure also shows the good resolution of the accelerator.

of the $(p,p_1\gamma)$ angular distribution for resonance $9A$ measured in this valley (Fig. 5) showed that about 38% of the measured $(p,p_1\gamma)$ yield originated from this $g_{9/2}$ fragment.

3. Resonances at $E_p = 3.1789$ MeV (resonance 11A), $E_p = 3.2326$ MeV (resonance 18A), $E_p = 3.2756$ MeV (resonance 27), and $E_p = 3.2975$ MeV (resonance 29)

To analyze the $(p,p_1\gamma)$ angular distributions measured on these resonances, similar procedures were carried out as was used for resonance $9A$.

4. Resonances at $E_p = 3.1922$ MeV (resonance 13A), $E_p = 3.2355$ MeV (resonance 19), and $E_p = 3.3362$ MeV (resonance 36)

Results of the analyses of $(p,p_1\gamma)$ angular distributions measured on these resonances showed that the main $g_{9/2}$ components were mixed with states of spin $\frac{1}{2}$.

5. $E_p = 3.2591$ MeV, resonance 24A

The $(p,p_1\gamma)$ angular distribution and its analysis based on Eq. (1) indicated the presence of a $J_R = \frac{7}{2}$ resonance (Fig. 13). However, neither $\frac{7}{2}^-$ nor $\frac{7}{2}^+$ parent states have been reported in this energy region. The likelihood of having $\frac{7}{2}^+$ resonances here is also rather low from shell model considerations. Furthermore, the $(p,p_1\gamma)$ angular distribution for a $\frac{7}{2}^+$ resonance is presumably complex [see Eq. (3)] giving a pattern far different from the measured one. The repeated excitation function measurement in 600 eV steps (Fig. 14) shows that there are at least two resonances (resonances $24A$ and 24) spaced about 800 eV apart, but resonance $24A$ is much stronger in the $(p,p_2\gamma)$ channel than in channel $(p,p_1\gamma)$. To clarify this case, we measured the *excitation function of angular distributions* as shown in Fig. 15. The angular distribution at the low energy tail has the pattern of spin $\frac{9}{2}$. At higher energy [nuclear magnetic resonance (NMR) frequency] the angular distribution pattern changes into a clear $\frac{5}{2}^+$ form.

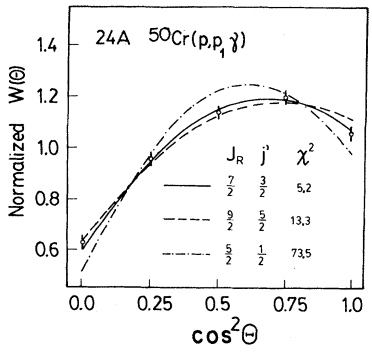

FIG. 13. Measured $(p,p_1\gamma)$ angular distribution on resonance $24A$ and the best fits with different spin assumptions.

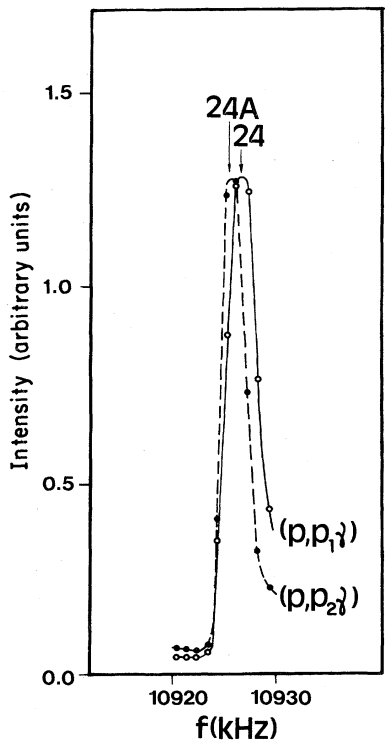

FIG. 14. Differential excitation functions for the ^{50}Cr(p,p$_1\gamma$) and ^{50}Cr(p,p$_2\gamma$) reactions measured in 600 eV steps in the vicinity of resonance 24.

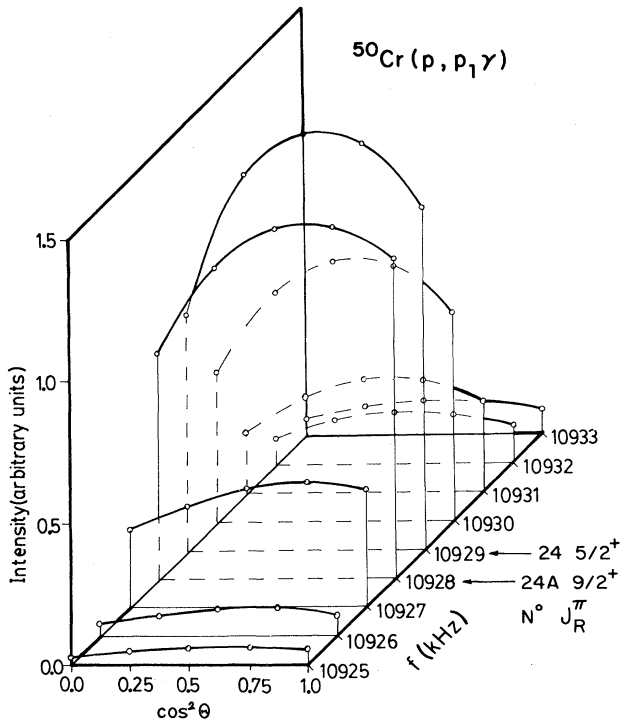

FIG. 15. Excitation function of the (p,p$_1\gamma$) angular distribution in the vicinity of resonance 24. For the sake of clarity the fitted angular distributions are shown. The fitted curves were always within the experimental errors, which varied between 1% (on top) and 5% (on the wings).

From the above we conclude that resonance 24A is $\frac{9}{2}^+$ [this is also supported by the measured (p,p$_2\gamma$) angular distribution shown in Fig. 8] and resonance 24 has spin parity $\frac{5}{2}^+$. Angular distribution analysis based on Eq. (4) yielded about 26% of the total (p,p$_1\gamma$) intensity measured on resonance 24A to be $\frac{5}{2}^+$.

6. Resonances at $E_p=3.2461$ MeV (resonance 21), $E_p=3.2662$ MeV (resonance 25), $E_p=3.3506$ MeV (resonance 38), and $E_p=3.3512$ MeV (resonance 39)

These resonances showed clear $\frac{9}{2}^+$ shape and thus were analyzed with the aid of Eq. (1).

Based on the distribution of the 15 fragments we considered resonances at $E_p=3.1403$, 3.1665, 3.1723, 3.1787, and 3.1922 MeV as belonging to the parent state at $E_x=4.101$ MeV and resonances at $E_p=3.2326$, 3.2355, 3.2461, 3.2586, 3.2662, 3.2756, 3.2925, 3.3362, 3.3506, and 3.3512 MeV as the fragments of the higher $\frac{9}{2}^+$ parent state at $E_x=4.155$ MeV.

C. The partial strengths of the resonances in the different channels

From the above measurements one may extract the quantities $\Gamma_p\Gamma_i/\Gamma$ for each resonance fragment, where $i=p_1$ or p_2 and $\Gamma=\Gamma_p+\Gamma_{p_1}+\Gamma_{p_2}$. Unfortunately, the elastic partial widths could not be measured directly. In order to deduce the elastic partial widths, the spectroscopic factors of the parent states were used, by taking

$$S_n=S_{pp}=(2T_0+1)\sum\Gamma_p/\Gamma_{s.p.}\ , \tag{6}$$

where T_0 is the isospin of the target nucleus, $\sum\Gamma_p$ stands for the sum of the elastic partial widths for the IAR, and $\Gamma_{s.p.}$ is the single-particle width calculated with program HANS.[25] For a meaningful correspondence of S_n and S_{pp}, the potential parameters for the proton single-particle calculations were the same as those used for the neutron potential in the DWBA calculations.[8,9,26]

The sums of the partial widths were calculated from Eq. (6) for both of the $\frac{9}{2}^+$ IAR's. These total strengths were then distributed among the fragments in accordance with their intensities in populating the $E_x=0.238$ MeV ($\frac{7}{2}^-$) first excited state which has strong single-particle character. With the aid of these semiempirical elastic partial widths, the corresponding Γ_{p_1} and Γ_{p_2} inelastic partial widths were calculated for each of the $\frac{9}{2}^+$ fragments. The results are shown in Table III.

The quantities $\Gamma_p\Gamma_i/\Gamma$ have errors of about 3—10%. The uncertainties of the partial width are estimated to be about 10—35% mainly due to errors in deriving the elastic widths. The errors for the reduced partial widths may be even larger because of the inaccuracy in the absolute value of the penetration factors. The distributions and the cumulative plots of the partial widths in different channels are shown in Fig. 16.

TABLE III. Partial and reduced widths for the fragments of the $g_{9/2}$ IAR's found in the ^{50}Cr(p,p), ^{50}Cr(p,p$_1$), and ^{50}Cr(p,p$_2$) reactions.

No.	E_p (MeV)	Γ_p[a] (eV)	γ_p^2 (keV)	$\frac{\Gamma_p\Gamma_{p_1}}{\Gamma}$[b] (eV)	Γ_{p_1} (eV)	$\gamma_{p_1}^2$ (keV)	$\frac{\Gamma_p\Gamma_{p_2}}{\Gamma}$[b] (eV)	Γ_{p_2} (eV)	$\gamma_{p_2}^2$ (keV)
5*A*	3.1403	1.30	0.79	0.70	1.54	0.10	0.008	0.02	0.04
8	3.1665	2.10	1.14	0.63	0.91	0.05	0.019	0.03	0.04
9*A*	3.1723	3.00	1.60	1.63	4.31	0.24	0.235	0.62	0.97
11*A*	3.1787	0.70	0.36	0.48	1.65	0.09	0.016	0.06	0.08
13*A*	3.1922	1.30	0.66	0.71	1.68	0.09	0.039	0.09	0.12
18*A*	3.2326	2.80	1.33	1.40	2.82	0.13	0.011	0.02	0.02
19	3.2355	2.60	1.18	1.25	2.43	0.11	0.011	0.02	0.02
21	3.2461	5.50	2.39	4.04	17.33	0.73	0.174	0.75	0.68
24*A*	3.2586	8.90	3.71	8.27	175.24	7.12	0.210	4.45	3.71
25	3.2662	11.00	4.51	2.72	3.62	0.15	0.018	0.24	0.19
27	3.2756	2.20	0.88	0.72	1.07	0.04	0.003	0.01	0.01
29	3.2925	3.20	1.23	1.59	3.18	0.11	0.009	0.02	0.01
36	3.3362	2.50	0.83	0.65	0.89	0.03	0.019	0.03	0.01
38	3.3506	2.60	0.84	0.99	1.63	0.05	0.027	0.04	0.02
39	3.3512	2.30	0.74	0.70	1.01	0.03	0.012	0.02	0.01

[a]Estimated.
[b]Measured.

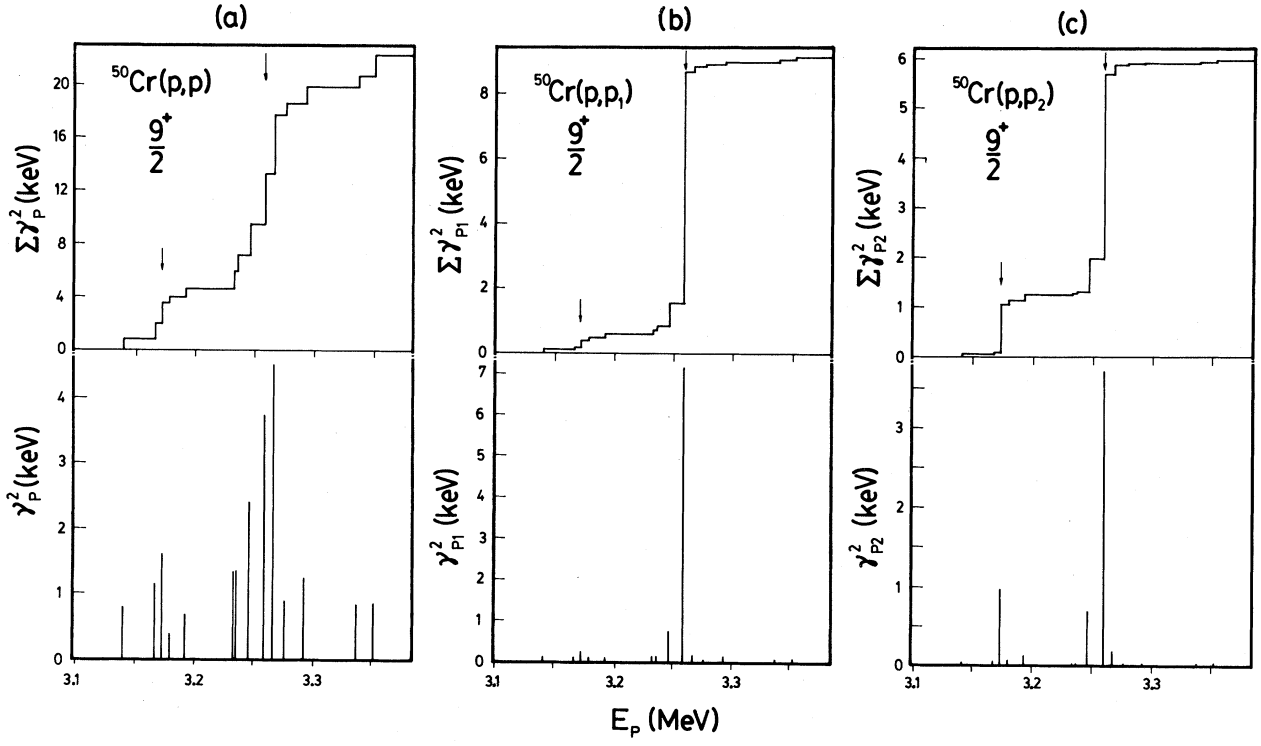

FIG. 16. Distribution and cumulative sum of the reduced partial widths in the elastic (a), first inelastic (b), and second inelastic (c) channels. The elastic widths are indirectly measured values (see the text for details). The cumulative sum shows two rises, indicated by arrows; however, they are not really steep in the elastic channel. The positions of the $g_{9/2}$ IAR's are most clearly shown by the sharper rises in the (p,p$_2$) channel.

D. Inelastic spectroscopic factors

The appearance of the $\frac{9}{2}^+$ resonance in the inelastic channels strongly suggests that the wave functions of these analog fragments contain non-negligible contributions from the wave functions of the two excited states of the ^{50}Cr target nucleus. It seems reasonable to assume that the parent states can be described in terms of a single neutron in a certain orbit coupled to the ground state and to the first and second core-excited states of the target nucleus. The inelastic spectroscopic factors corresponding to these terms give the measure of how important these inelastic terms are in the formation and decay of different IAR's.

From the sums of the inelastic partial widths, inelastic spectroscopic factors were obtained using the same relation [Eq. (6)] from which the elastic partial widths were derived, except that for the inelastic single-particle widths the energies and angular momenta were those of the inelastically scattered protons. The inelastic spectroscopic factors for the two $g_{9/2}$ IAR's are listed in Table IV. The values by the Thomson-Adams-Robson (TAR) method are larger than the ones calculated with the Zaidi-Darmodjo-Harvey (ZDH) or Mekjian-MacDonald (MM) method (for details on those, see the papers listed in Ref. 25). However, the values are large especially for the stronger IAR, thus giving evidence of the important role of core excitations in the wave functions of the analog and parent states.

V. THE FINE STRUCTURE ANALYSES

The distributions of the reduced partial widths of the $\frac{9}{2}^+$ fragments showed different patterns in the different channels (see Fig. 16). In channels (p,p$_1$) and (p,p$_2$) the strengths are concentrated into one or two intense levels, while in the elastic channel the strengths are more evenly distributed among the fragments. For more quantitative results, fine structure analyses were performed by the method of MacDonald-Mekjian-Kerman-De Toledo Piza[27,28] (MMKP), because this method seemed to give reasonable results independently of the number of fragments, even for numbers with low statistical significance, i.e., five and ten for the lower and higher $g_{9/2}$ IAR's, respectively.

The Lorentz-weighted average of the experimental reduced partial widths (γ_λ^2) (i.e., the smooth "experimental" strength function):

$$S(E;I)=\langle\gamma_\lambda^2/D_\lambda\rangle=\frac{I}{\pi}\sum_\lambda\frac{\gamma_\lambda^2}{(E-E_\lambda)^2+I^2}\ , \tag{7}$$

where D_λ is the mean level spacing and I is the width of Lorentz weight of averaging, was least-squares fitted to the parametric form of the doorway strength function:[29]

$$S^D(E;I)=S_0+\frac{1}{\pi}\frac{\gamma_A^2}{\cos^2\phi}\frac{\left[I+\frac{\Gamma_s}{2}\right]\cos2\phi-(E-\hat{E}_A)\sin2\phi}{(E-\hat{E}_A)^2+\left[I+\frac{\Gamma_s}{2}\right]^2}, \tag{8}$$

where S_0 stands for the background strength function, γ_A^2 is the analog state total reduced width, Γ_s is the spreading width (the parameter that measures the strength of the spreading and depends directly on the mean value of the doorway-hallway coupling matrix elements;[29] this coupling of the doorway state to more complicated hallway states makes the doorway state share its strength among the hallway states), and $\hat{E}_A=E_A+\Delta_A$ is the analog state energy containing the analog shift Δ_A arising also from the doorway-hallway coupling. Usually Δ_A is considered to be negligible. The parameter ϕ describes the asymmetry of the strengths around the position of the analog state.

The fitting procedures for the (p,p), (p,p$_1$), and (p,p$_2$) channels were carried out independently and repeated with increasing averaging widths I, until the resulting fine structure parameters became independent of the value of I itself.

The results of the analyses are listed in Table V. The distribution of the original partial widths together with the final fitted strength functions are shown in Figs. 17 and 18 for the two $g_{9/2}$ IAR's.

Due to the uncertainties in the values of the partial widths, special attention was paid to see how the errors of the derived fine structure parameters depend on the magnitude of the errors of the initial partial widths. The details along with discussion of the propagation of errors through a fine structure analysis of the MMKP-type are presented in the Appendix.

VI. DISCUSSION AND CONCLUSIONS

A. Comparison with other measurements

1. *Resonance energies and spins*

Due to the high sensitivity of our method and the selectivity of the (p,p$_2$) reaction for higher spin resonances, even weak resonances could be identified. These high spin

TABLE IV. Elastic and inelastic spectroscopic factors for the two $1g_{9/2}$ IAR's in ^{51}Mn. For details on differences in the values of the spectroscopic factors derived by different methods see references given in Ref. 25.

E_x^{parent}		S_{pp_1}			S_{pp_2}		
(MeV)	S_n	(TAR)	(ZDH)	(MM)	(TAR)	(ZDH)	(MM)
4.101	0.10	0.012	0.009	0.009	0.014	0.008	0.008
4.155	0.34	0.187	0.149	0.146	0.051	0.029	0.029

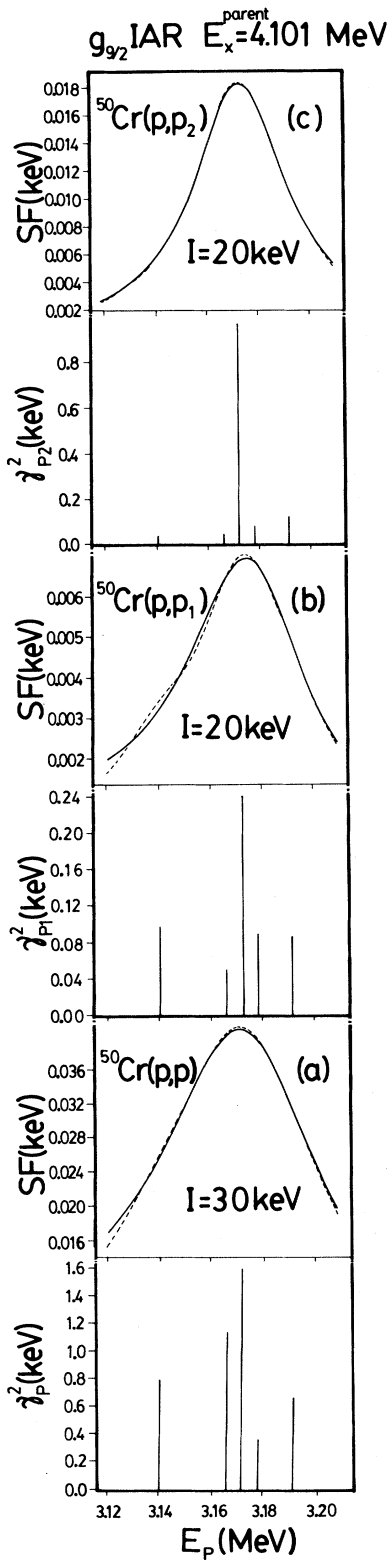

FIG. 17. Distribution of the partial widths and the fitted strength functions for the lower $g_{9/2}$ IAR in ^{51}Mn (E_x^{parent}=4.101 MeV) in channels (p,p) (a), (p,p$_1$) (b), and (p,p$_2$) (c). The full curves are the five parameter theoretical strength functions of the MMKP-type (see the text for further details). The broken lines are the Lorentz-averaged (of half-width I) experimental strength functions.

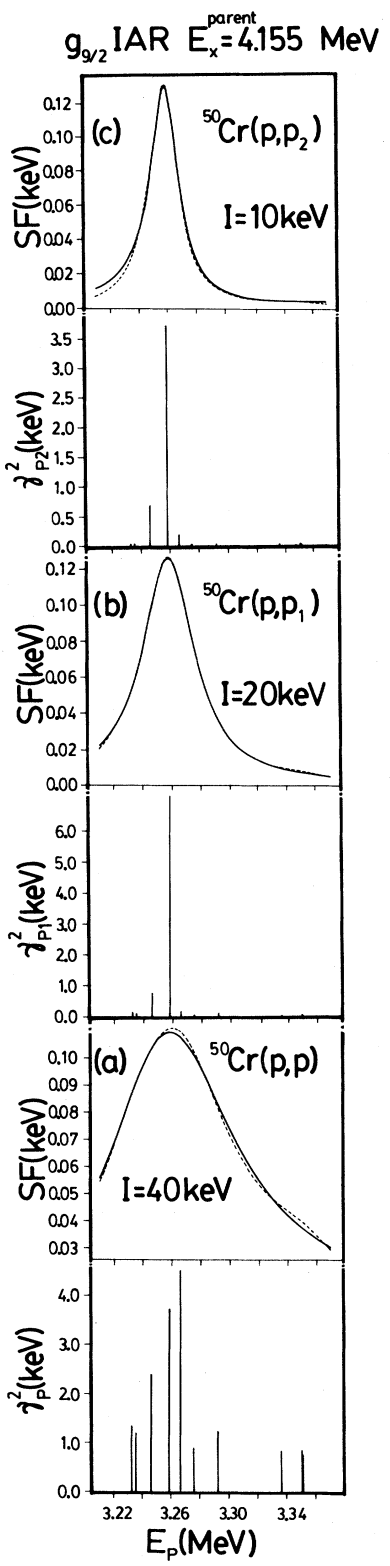

FIG. 18. Distribution of the partial widths and the fitted strength functions for the higher $g_{9/2}$ IAR in ^{51}Mn (E_x^{parent}=4.155 MeV) in channels (p,p) (a), (p,p$_1$) (b), and (p,p$_2$) (c). Details as in Fig. 17.

TABLE V. Fine structure parameters for the $1g_{9/2}$ IAR's in ^{51}Mn for the ^{50}Cr(p,p), ^{50}Cr(p,p$_1$), and ^{50}Cr(p,p$_2$) reaction channels.

E_x^{parent} (MeV)		(p,p)	(p,p$_1$)	(p,p$_2$)
4.101(10)	E_A (MeV)	3.174(3)	3.176(3)	3.173(2)
	S_0 (keV)	0.004(2)	0.002(2)	0.001(1)
	γ_A^2 (keV)	4.543(11)	0.571(3)	1.250(3)
	Γ_s (keV)	11.2(3.0)	14.0(2.8)	4.4(1.4)
	tanϕ	0.050(40)	0.070(20)	0.002(4)
	I (keV)	30	20	20
4.155(10)	E_A (MeV)	3.252(5)	3.257(3)	3.257(3)
	S_0 (keV)	0.003(2)	0.001(2)	0.002(2)
	γ_A^2 (keV)	17.640(8)	8.500(6)	4.686(4)
	Γ_s (keV)	24.2(1.8)	2.6(8)	2.2(8)
	tanϕ	−0.147(24)	−0.006(4)	0.006(5)
	I (keV)	40	20	10

TABLE VI. Present results and their comparison with others.

No.	E_p (MeV)	J_R^π	E_x (MeV)	E_p[h] (Ref. 3) (MeV)	J_R^π (Refs.)	
1A	3.0991	$\frac{1}{2}+\frac{5}{2}^{(-)}$	8.3091			
1B	3.1013	$\frac{3}{2}^{(-)}$	8.3113			
				3.1025	$\frac{1}{2}^{+}$[a]	
2	3.1150	$\frac{3}{2}^{-}$	8.3247	3.1145	$\frac{3}{2}^{-}$[b,f]	$\frac{1}{2}^{-}$[a]
3	3.1196	$\frac{1}{2}^{-}$	8.3292	3.1195	$\frac{1}{2}^{-}$[a]	
				3.1244	$\frac{5}{2}^{-}$[a]	
4	3.1307	$\frac{5}{2}^{+}$	8.3401	3.1307	$\frac{5}{2}^{+}$[a]	
5	3.1395	$\frac{3}{2}^{(-)}$	8.3487	3.1393	$\frac{5}{2}^{+}$[a]	
5A	3.1403	$\frac{9}{2}^{+}$	8.3495			
6	3.1485	$\frac{5}{2}^{+}$	8.3576	3.1482	$\frac{5}{2}^{+}$[a]	
7	3.1538	$\frac{5}{2}^{+}$	8.3628	3.1538	$\frac{5}{2}^{+}$[a]	
				3.1612	$\frac{1}{2}^{+}$[e]	
8	3.1665	$(\frac{9}{2}^{+})$	8.3752			
9	3.1712	$\frac{3}{2}^{-}$	8.3798	3.1705	$\frac{3}{2}^{-}$[b,f]	$\frac{1}{2}^{-}$[a]
9A	3.1723	$\frac{9}{2}^{+}$	8.3809			
				3.1739	$\frac{3}{2}^{-}$[b,f]	$\frac{1}{2}^{-}$[a]
10	3.1747	$\frac{5}{2}^{+}+\frac{1}{2}$	8.3833			
11A	3.1789	$\frac{9}{2}^{+}$	8.3874			
11	3.1808	$\frac{3}{2}^{(+)}$	8.3892			
12	3.1828	$\frac{5}{2}^{-}$	8.3912	3.1826	$\frac{5}{2}^{-}$[c]	$\frac{5}{2}^{+}$[a]
13A	3.1922	$\frac{9}{2}^{+}$	8.4004			
13	3.1946	$\frac{1}{2}$	8.4028	3.1944	$\frac{3}{2}^{-}$[b,f]	$\frac{1}{2}^{-}$[a]
				3.1973	$\frac{5}{2}^{+}$[a,e]	
14	3.1981	$\frac{3}{2}^{(-)}$	8.4062			
15	3.2004	$\frac{5}{2}^{+}$	8.4084	3.1999	$\frac{5}{2}^{+}$[a,e]	
16	3.2150	$\frac{3}{2}^{(-)}$	8.4228			

TABLE VI (*Continued*).

No.	E_p (MeV)	J_R^π	E_x (MeV)	E_p[h] (Ref. 3) (MeV)	J_R^π (Refs.)	
17	3.2227	$\frac{1}{2}(\frac{3}{2}^-)$	8.4303	3.2221	$\frac{3}{2}^-$ a,d,f	$\frac{1}{2}^-$ e
18	3.2320	$\frac{3}{2}^{(-)}$	8.4394			
18*A*	3.2326	$(\frac{9}{2}^+)$	8.4400	3.2331	$\frac{5}{2}^+$ a	$\frac{1}{2}^+$ e
19	3.2355	$\frac{9}{2}^+ + \frac{1}{2}$	8.4429			
20	3.2444	$(\frac{5}{2}^-)$	8.4516			
21	3.2461	$\frac{9}{2}^+$	8.4533	3.2461	$\frac{9}{2}^+$ c,d,e	
22	3.2503	$\frac{3}{2}^{(-)}$	8.4574			
23	3.2523	$\frac{1}{2}^+ + (\frac{5}{2}^-)$	8.4593			
24*A*	3.2586	$\frac{9}{2}^+$	8.4655	3.2586	$\frac{9}{2}^+$ c,d	$\frac{5}{2}^+$ a,e
24	3.2595	$\frac{5}{2}^+$	8.4664	3.2594	$\frac{5}{2}^+$ a,c,d,g	
				3.2637	$\frac{1}{2}^+$ c,d	
25	3.2662	$\frac{9}{2}^+$	8.4730	3.2662	$\frac{9}{2}^+$ c,e	$\frac{5}{2}^+$ a,d
26	3.2692	$\frac{3}{2}^- + (\frac{5}{2}^-)$	8.4759	3.2692	$\frac{3}{2}^-$ c,d,e,f	$\frac{1}{2}^-$ a
27	3.2756	$\frac{9}{2}^+ + \frac{3}{2}^{(-)}$	8.4822			
28	3.2863	$\frac{5}{2}^+$	8.4927	3.2867	$\frac{5}{2}^+$ a,d,e,g	
29	3.2925	$\frac{9}{2}^+ + \frac{3}{2}^-$	8.4987	3.2923	$\frac{3}{2}^-$ d,f	$\frac{5}{2}^+$ a
30	3.2946	$\frac{5}{2}^+$	8.5008	3.2946	$\frac{5}{2}^+$ c,d,e,g	
31	3.2981	$\frac{1}{2}^- + \frac{5}{2}^+$	8.5042	3.2980	$\frac{1}{2}^-$ a,d,e	$\frac{3}{2}^-$ c
32	3.3065	$\frac{3}{2}^{(+)}$	8.5125			
33	3.3148	$(\frac{5}{2}^-, \frac{7}{2}^-)$	8.5206	3.3149	$\frac{5}{2}^-$ d	
34	3.3207	$\frac{1}{2}^+ + \frac{5}{2}^+$	8.5264	3.3208	$\frac{1}{2}^+$ c,d,e	
35	3.3315	$\frac{5}{2}^{(-)}$	8.5370	3.3323	$\frac{5}{2}^-$ d	
36	3.3362	$\frac{9}{2}^+ + \frac{1}{2}$	8.5416			
37	3.3446	$\frac{3}{2}^+$	8.5498	3.3454	$\frac{3}{2}^-$ c,d,e,f	
38	3.3506	$\frac{9}{2}^+$	8.5557			
38*A*	3.3512	$\frac{9}{2}^+$	8.5563			

[a]Reference 1.
[b]Reference 2.
[c]Reference 3.
[d]Reference 4.
[e]Reference 5.
[f]Reference 6.
[g]Reference 7.
[h]For the sake of clarity, all proton energies measured in different laboratories (and different from each other in absolute value) were converted into the energy scale measured at Zürich (Ref. 3). Using this scale, the relative error on our energies is about 800 eV.

resonances remained unobserved or were not analyzed in the proton scattering measurements.[1-5] However, the energies and the extracted spins in the present work show excellent agreement with those found in the recent studies.[3-7] Comparison of the present results with those of the other studies is shown in Table VI.

Differences or disagreements, mainly for the $g_{9/2}$ fragments, could arise from the difference in the sensitivities of the methods employed. The derived partial widths (see Table III), except for the stronger fragments, are near or below the lower limit of the usual sensitivity of the proton scattering experiments.[3]

2. *Partial and reduced widths*

A detailed comparison, made only for the three earlier identified $\frac{9}{2}^+$ fragments at $E_p = 3.2461$, 3.2586, and 3.2662 MeV and only for the elastic and first inelastic partial widths, is given in Table VII. Taking into account the large uncertainties in the values of the partial widths, the results are not contradictory. However, our elastic partial widths, except for the fragment at $E_p = 3.2664$ MeV, are smaller than that of the earlier works. If the neutron spectroscopic factors were calculated from the Γ_p values of Ref. 3, they would exceed the measured S_n

TABLE VII. Comparison of the partial widths for the elastic and first inelastic channels found in different laboratories.

	Present results				Zürich 1977 (Ref. 3)				Tokyo 1983 (Ref. 5)		
E_p (MeV)	Γ_p (eV)	γ_p^2 (keV)	Γ_{p_1} (eV)	$\gamma_{p_1}^2$ (keV)	Γ_p (eV)	γ_p^2 (keV)	Γ_{p_1} (eV)	$\gamma_{p_1}^2$ (keV)	Γ_p (eV)	γ_p^2 (keV)	Γ_{p_1} (eV)
3.2461	5.5	2.4	17.3	0.73	10.0	13.0	30.0	3.4	8.8	4.4	12.0
3.2587	8.9	3.7	175.2	7.12	18.0	23.0	36.0	3.9	$\frac{5}{2}^+$		
3.2664	11.0	4.5	3.6	0.15	8.0	10.0	12.0	1.3	6.4	3.32	9.6

values by a factor of 2 or more. The large disagreements in the orders of magnitude of the reduced partial widths probably originate from differences in the penetration factors used in different laboratories.

3. *Comparison of the Coulomb displacement energies*

The experimental Coulomb displacement energies are deduced from the positions of the corresponding parent and analog states and are, therefore, very sensitive to the selection of the corresponding states. Special problems can occur, as in our case, when the parents of the same type are so closely spaced that it is really hard to tell which analog fragment belongs to which parent state. Depending on this selection, the Coulomb energy values can easily differ from each other. Another source for error can arise from the derivation of the centroid of the analog. The case becomes easier when fine structure analysis can be made, because the most reliable parameter extracted from such analysis is the position of the analog state.

From the positions of the analog states, given in Table V, the Coulomb displacement energies were calculated for both $g_{9/2}$ IAR's. In Table VIII, they are listed and compared with values from other works.[3,5] The discrepancy for the lower IAR is mainly due to differences in the identification of the analog states.

B. Spreading patterns in different channels for the two $g_{9/2}$ IAR's

Table V lists the fine structure parameters for both of the $g_{9/2}$ IAR's in all three decay channels. The following can be stated:

(i) In spite of having made the fits of fine structure analysis independently in the three channels, the parameters are in good agreement except for the values for the spreading widths and the asymmetry angles.

(ii) The background strength functions are very weak in all cases.

TABLE VIII. Comparison of the Coulomb displacement energies.

E_x (MeV)	Present work ΔE_C (MeV)	Zürich 1977 (Ref. 3) ΔE_C (MeV)	Tokyo 1983 (Ref. 5) ΔE_C (MeV)
4.101	8.273+0.015		8.339
		8.311	
4.155	8.299+0.015		8.308

(iii) The positions of the IAR's are the same within the errors in all three channels.

(iv) The total reduced widths are reasonably well reproduced for all cases.

(v) The changes in the value and sign of the asymmetry angles from channel to channel for the two IAR's are non-negligible. This is hard to explain on the basis of the theory (see Refs. 27–29 and references therein).

(vi) The spreading width for the lower IAR is about the same for the (p,p) and (p,p_1) channels, but the width is considerably smaller in the (p,p_2) channel. For the higher IAR the spreading width in the elastic channel is about eight times larger than in the (p,p_1) and (p,p_2) channels. A similar case was reported for the $\frac{3}{2}^-$ IAR in ^{49}V by Bilpuch *et al.*[30] but no satisfactory explanation has been suggested. However, due to the uncertainties already mentioned and the relatively low number of fragments, we may not draw serious conclusions regarding the spreading patterns in different channels. Without detailed analysis, and based only on the distributions of the partial widths (Figs. 16–18), it seems that while the lower IAR in channel (p,p_2) and the higher IAR in channels (p,p_1) and (p,p_2) look like good examples for the "weak mixing" (see, e.g., in Ref. 30), the lower IAR in channels (p,p) and (p,p_1) and the higher IAR in the elastic channel appear to demonstrate "intermediate mixing." We may take this to mean that the spreading in different channels is really different.

Further evidence can be derived by considering those values of the half-width I of the Lorentz averaging, for which the fine structure parameters became independent of the I values themselves and the fits were stopped. The stronger the spreading, the larger I was necessary to take into account the effects of the further-lying fragments. In other words, if the doorway-hallway coupling is strong (large spreading width) it can effectively couple further-lying hallway states to the doorway (analog) state as well. If it is weak, only the close-lying hallway levels can share some of the analog strength. In the case of the higher $\frac{9}{2}^+$ IAR in the elastic channel [see Fig. 18(a)] the analog strength is distributed almost evenly among the fragments. For this case $I=40$ keV averaging was necessary to make the parameters independent of I. The opposite example is given by the same IAR in the (p,p_2) channel, where $I=10$ keV made the parameters independent of I.

In spite of the above-mentioned uncertainties in the values of the reduced partial widths, the present results suggest that further theoretical studies are needed regarding the correctness of the independent fine structure analyses in different channels and the probable explanations for the different spreading patterns in these channels.

TABLE IX. Dependence of the values and errors of the fine structure parameters for the higher $1g_{9/2}$ IAR in ^{51}Mn, on the uncertainties of the initial experimental partial width in a fine structure analysis of the MMKP-type.

	Relative errors			
Top	8%	16%[a]	32%	64%
Wings	80%	160%	300%	600%
E_A (keV)	3257±0.5	3257±0.6	3257±0.7	3257±0.9
S_0 (eV)	0.28±0.09	0.24±0.15	0.26±0.32	0.24±0.44
γ_A^2 (keV)	4.686±0.003	4.686±0.004	4.686±0.004	4.686±0.005
Γ_s (keV)	2.2±0.4	2.2±0.8	2.2±2.0	2.4±3.4
tanϕ	0.003±0.003	0.005±0.006	0.004±0.011	0.005±0.014

[a]These errors are considered realistic for the actual case.

However, further experiments on other nuclei regarding the role of the different core excited states of the target nuclei in the formation and decay of different IAR's would give an incentive for such theoretical studies.

ACKNOWLEDGMENTS

The authors would like to thank V. Janzen, Y. Leclerc, and R. Schubank for their assistance in performing the measurements and the operation staff for the excellent operation of the Van de Graaff accelerator at Université Laval. The helpful discussions with Professor G. E. Mitchell, his critical remarks, and his assistance in making available proton scattering data on ^{50}Cr prior to publication are greatly appreciated. This research was supported by grants from the Natural Sciences and Engineering Research Council of Canada.

APPENDIX: PROPAGATION OF ERRORS IN FINE STRUCTURE ANALYSIS

Because of the nonlinear nature of the propagation of errors in a fine structure analysis of the MMKP-type, it is hard to predict the uncertainties of the fine structure parameters arising from the errors of the initial experimental strengths. The major source of this uncertainty comes from the incomplete knowledge of the errors of the smooth "experimental" strength function which is derived from the experimental partial widths with the aid of Eq. (7).

If the fit is made in the energy interval $E_{\text{initial}} < E_i < E_{\text{final}}$ ($i=1-100$ in the present case), the value of the smooth energy-averaged strength function in the ith point is

$$y_i \equiv S(E_i,I) = \frac{I}{\pi}\sum_\lambda \frac{\gamma_\lambda^2}{(E_i-E_\lambda)^2+I^2} = \sum_\lambda C_\lambda(E_i,I)\gamma_\lambda^2 , \tag{A1}$$

where γ_λ^2 are the measured strengths with errors σ_λ, and

$$C_\lambda(E,I) = \frac{I}{\pi}\frac{1}{(E-E_\lambda)^2+I^2} \equiv \frac{\partial y_i}{\partial(\gamma_\lambda^2)} . \tag{A2}$$

The errors of the smooth experimental strength function are given by the square root of the variances σ_i^2 for y_i (see, e.g., Ref. 31):

$$\sigma_i^2 = \sum_\lambda \left\{ \sigma_\lambda^2 \left[\frac{\partial y_i}{\partial(\gamma_\lambda^2)} \right]^2 + \sum_\mu \sigma_{\lambda\mu}^2 \left[\frac{\partial y_i}{\partial(\gamma_\lambda^2)} \right] \left[\frac{\partial y_i}{\partial(\gamma_\mu^2)} \right] \right\} . \tag{A3}$$

If the experimental errors σ_λ were completely correlated, then the covariances in Eq. (A3) would make σ_i vanish, giving no errors at all, for the energy-averaged strength function.

To estimate upper limits for these errors, we suppose that the experimental errors σ_λ are uncorrelated, so that the second term in Eq. (A3) containing the covariances can be neglected. Then,

$$\sigma_i^2 = \sum_\lambda \sigma_\lambda^2 \left[\frac{\partial y_i}{\partial(\gamma_\lambda^2)} \right]^2 = \sum_\lambda \sigma_\lambda^2 C_\lambda^2(E_i,I) . \tag{A4}$$

Thus the errors for the smooth experimental strength function are given by

$$\sigma_i = \left[\sum_\lambda C_\lambda^2(E_i,I)\sigma_\lambda^2 \right]^{1/2} . \tag{A5}$$

Any existing correlation, however, among the errors σ_λ can reduce the variance σ_i^2 through the second term in Eq. (A3).

It is evident from Eqs. (A1)–(A5) that these variances, affecting directly the evaluation of the χ^2 in the fitting procedure, depend on the size of the averaging interval I as well. Thus for the analyses these variances σ_i^2 were calculated together with the energy averaging when the smooth experimental strength functions were derived. For quantitative results, fine structure analyses were carried out on the fragments of the higher $1g_{9/2}$ IAR in

^{51}Mn in the (p,p$_2$) channel considering increasing experimental errors for the partial widths. The results are shown in Table IX.

As can be seen from Table IX, the sensitivity of the errors of various parameters for increasing input errors are quite different. The extremely large initial errors cause considerable increase in the errors of parameters S_0 and $\tan\phi$; however, the error of Γ_s is increased from $\sim 18\%$ up to "only" $\sim 140\%$, while the increase of errors of parameters E_A and γ_A^2 are almost negligible.

These results suggest that the analyses performed with errors derived from Eq. (A5) with realistic initial errors σ_λ supply a reliable set of parameters characterizing the fragmentation.

---

*Permanent address: Central Research Institute for Physics, Budapest 114, P.O. Box 49, Hungary, H-1525.

[1]J. D. Moses, E. G. Bilpuch, H. W. Newson, and G. E. Mitchell, Nucl. Phys. **A175**, 556 (1971).

[2]T. R. Dittrich, C. R. Gould, and G. E. Mitchell, Nucl. Phys. **A279**, 430 (1977).

[3]M. Salzmann, V. Meyer, and H. Brändle, Nucl. Phys. **A282**, 317 (1977).

[4]K. M. Whatley, C. R. Westerfeldt, E. G. Bilpuch, and G. E. Mitchell, Bull. Am. Phys. Soc. **27**, 497 (1982); K. M. Whatley, Ph.D. dissertation, Duke University, 1982.

[5]E. Arai, M. Futakuchi, J. Komaki, M. Ogawa, and Y. Oguri, J. Phys. Soc. Jpn. **42**, 802 (1983).

[6]J. F. Shriner, Jr., K. M. Whatley, E. G. Bilpuch, C. R. Westerfeldt, and G. E. Mitchell, Z. Phys. A **313**, 51 (1983).

[7]K. M. Whatley, E. G. Bilpuch, G. E. Mitchell, J. F. Shriner, Jr., and C. R. Westerfeldt, J. Phys. G **9**, 1527 (1983).

[8]A. E. McGregor and G. Brown, Nucl. Phys. **A190**, 548 (1972).

[9]J. E. Robertshaw, S. Mecca, A. Sperduto, and W. W. Buechner, Phys. Rev. **170**, 1013 (1968).

[10]I. Fodor, I. Szentpétery, and J. Szücs, Phys. Lett. **32B**, 689 (1970).

[11]I. Szentpétery and Judit Szücs, Phys. Rev. Lett. **28**, 378 (1972).

[12]I. Fodor, J. Sziklai, B. Kardon, J. Rama Rao, K. Beckert, F. Herrmann, and H. Schobbert, J. Phys. G **4**, 1117 (1978).

[13]I. Fodor, J. Sziklai, P. Kleinwächter, H. Schobbert, and F. Hermann, J. Phys. G **5**, 1267 (1979).

[14]S. Galès, S. Fortier, H. Laurent, J. M. Maison, and J. P. Schapira, Nucl. Phys. **A265**, 213 (1976).

[15]S. Galès, S. Fortier, H. Laurent, J. M. Maison, and J. P. Schapira, Phys. Rev. C **14**, 842 (1976).

[16]S. Galès, S. Fortier, H. Laurent, J. M. Maison, and J. P. Schapira, Nucl. Phys. **A268**, 257 (1976).

[17]J. Rapaport, T. A. Belote, and W. E. Dorenbusch, Nucl. Phys. **A100**, 280 (1967).

[18]J. E. Park, W. W. Daehnick, and M. J. Spisak, Phys. Rev. C **19**, 42 (1979).

[19]E. K. Warburton and J. Weneser, in *Isospin in Nuclear Physics,* edited by D. H. Wilkinson (North-Holland, Amsterdam, 1969), p. 173.

[20]J. W. Noé, R. W. Zurmühle, and D. P. Balamuth, Nucl. Phys. **A277**, 137 (1977).

[21]E. Sheldon and D. M. van Patter, Rev. Mod. Phys. **38**, 143 (1966).

[22]K. S. Krane, Nucl. Instrum. Methods **98**, 205 (1972).

[23]J. A. Cameron and G. U. Din (unpublished).

[24]B. H. Chou, G. E. Mitchell, E. G. Bilpuch, and C. R. Westerfeldt, Z. Phys. A **300**, 157 (1981).

[25]H. L. Harney (unpublished). This program gives three different results corresponding to the three methods used: (i) W. J. Thompson, J. L. Adams, and D. Robson, Phys. Rev. **173**, 975 (1968), and referred to as method TAR; (ii) S. A. A. Zaidi and S. Darmodjo, Phys. Rev. Lett. **19**, 1445 (1967); H. L. Harney, C. A. Wiedner, and J. P. Wurm, Phys. Lett. **26B**, 204 (1968); H. L. Harney, Nucl. Phys. **A119**, 591 (1968), referred to as method ZDH; (iii) A. Mekjian and W. M. MacDonald, Nucl. Phys. **A121**, 385 (1968), and referred to as method MM.

[26]G. Brown, A. Denning, and A. E. McGregor, Nucl. Phys. **A153**, 145 (1970).

[27]W. M. MacDonald and A. Z. Mekjian, Phys. Rev. **160**, 730 (1967).

[28]A. K. Kerman and A. F. R. De Toledo Piza, Ann. Phys. (N.Y.) **48**, 183 (1968).

[29]W. M. MacDonald, Ann. Phys. (N.Y.) **125**, 253 (1980).

[30]E. G. Bilpuch, A. M. Lane, G. E. Mitchell, and J. D. Moses, Phys. Rep. **28**, 145 (1976).

[31]P. R. Bevington, *Data Reduction and Error Analysis in the Physical Sciences* (McGraw-Hill, New York, 1969), p. 59, Eqs. (4)—(8).